STORM imaging of mitochondrial dynamics using a vicinal-dithiol-proteins-targeted probe

Bingling Chen[a,1], Wanjun Gong[a,1], Zhigang Yang[a,**], Wenhui Pan[a], Peter Verwilst[b], Jinwoo Shin[b], Wei Yan[a], Liwei Liu[a], Junle Qu[a,***], Jong Seung Kim[a,b,*]

[a] *Key Laboratory of Optoelectronic Devices and Systems of Ministry of Education and Guangdong Province, College of Physics and Optoelectronic Engineering, Shenzhen University, Shenzhen, 518060, China*
[b] *Chemistry Department, Korea University, Seoul, 02841, Republic of Korea*

ARTICLE INFO

ABSTRACT

Stochastic optical reconstruction microscopy (STORM) is a promising method for the visualization of ultra-fine mitochondrial structures. However, this approach is limited to monitoring dynamic intracellular events owing to its low temporal resolution. We developed a new strategy to capture mitochondrial dynamics using a compressed sensing STORM algorithm following raw data pre-treatments by a noise-corrected principal component analysis and K-factor image factorization. Using STORM microscopy with a vicinal-dithiol-proteins targeting probe, visualizing mitochondrial dynamics was attainable with spatial and temporal resolutions of 45 nm and 0.8 s, notably, dynamic mitochondrial tubulation retraction of ~746 nm in 1.2 s was monitored. The labeled conjugate was observed as clusters (radii, ~90 nm) distributed on the outer mitochondrial membranes, not yet reported as far as we know. This strategy is promising for the quantitative analysis of intracellular behaviors below the optical diffraction limit.

1. Introduction

Mitochondria are characterized by highly interconnected networks and dynamic changes [1]. The formation and maintenance of mitochondrial networks are mediated by the fusion of individual mitochondria and junctions between tubules [2]. Dynamic changes in the fusion-fission balance and mitochondrial tubular network formation determine the overall morphology and biological behaviors of mitochondria. Furthermore, in a process referred to as dynamic tubulation, tubules stretch to fuse with the membranes of other mitochondria [3]. These dynamic events facilitate the maintenance of normal mitochondrial functions, such as the interchange of mitochondrial materials, DNA integrity, respiratory capacity, response to cellular stress, and apoptosis [4]. However, disruptions in mitochondrial dynamics lead to abnormal development and human diseases, including neurodegenerative disorders and cancers [5]. Therefore, investigations of mitochondrial dynamics are critical to enable a deeper understanding of diseases related to mitochondrial dysfunctions.

Fluorescence microscopy is widely used to investigate single mitochondria in live cells [6]. However, imaging mitochondrial substructures using conventional optical microscopy is limited by the optical diffraction limit. Since the emergence of super-resolution imaging, it has become feasible to visualize ultra-fine structures [7]. Stochastic optical reconstruction microscopy (STORM) has an outstanding imaging ability for biological objects below 200 nm in size [8]. Fluorescent probes composed of fluorophores (e.g., Alexa647) and antibodies are favored for STORM imaging in fixed cells [9,10]. However, live cell imaging by STORM remains challenging owing to the lack of appropriate probes and low temporal resolution. In particular, direct STORM has rarely been used to evaluate mitochondrial dynamics.

Smart fluorescent probes that selectively target mitochondrial membrane-bound proteins would facilitate the imaging of mitochondrial membrane structures using STORM. Mitochondria possess abundant vicinal dithiol proteins (VDPs) with two proximal cysteine residues in their primary structures; they play essential roles in maintaining mitochondrial redox homeostasis, antioxidant defense, and redox signaling. Fluorescent arsenicals contain a 1, 3, 2-dithiarsenolane moiety capable of selectively binding to VDPs by forming covalent bonds [11].

* Corresponding author.
** Corresponding author.;
*** Corresponding author.;
E-mail addresses: zhgyang@szu.edu.cn (Z. Yang), jlqu@szu.edu.cn (J. Qu), jongskim@korea.ac.kr (J.S. Kim).
[1] These authors contributed equally to this work.

They can label mitochondrial VDPs in situ, providing a basis for the application of STORM to mitochondria in live cells [12]. However, STORM involves sparse lighting and dilute labeling with fluorescent probes during sample preparation, and thousands of frames are needed to reconstruct a super-resolution image, resulting in poor temporal resolution [13,14]. Temporal resolution can be improved by reducing the number of frames. Compressed sensing STORM (CSSTORM) is an l_1-norm minimization-based multi-molecule localization algorithm and is more suitable for dense fluorescence than single-molecule fitting. It can substantially shorten the time required for signal acquisition by cutting the number of required frames, and the temporal resolution can be further improved by increasing the acquisition frame rate of the electron multiplying charge coupled device (EMCCD) [15]. However, the rapid signal acquisition will increase background noise, thereby increasing interference in image reconstruction. For the application of STORM to live cell mitochondrial dynamics, the development of smart probes targeting mitochondrial membrane VDPs with an improved reconstruction algorithm for noise suppression is a promising strategy.

In this work, we performed STORM imaging of mitochondrial dynamics in live cells, and carried out the quantitative analysis of the target under STORM super-resolution microscopy. A new fluorescent marker suitable for STORM imaging was developed to selectively label VDPs on the outer mitochondrial membrane by simple co-culturing with cells. Meanwhile, we employed a moderate illuminating laser power to obtain as much single-frame emitter localiztion as possible and to reduce photobleaching and phototoxicity. The temporal resolution of STORM imaging can be achieved by reducing the laser power and increasing the CCD frame rate. To avoid interference from background noises, a combination of noise-corrected principal component analysis (NC-PCA) and K-factor image factorization were developed to treat the raw data prior to reconstruction using the CSSTORM algorithm. The principle and implementation of the algorithms were further described in the Supplemental Information (Figs. S14–S17). Using this strategy, we achieved STORM imaging of mitochondrial dynamics including fusion, fission, and mitochondrial tubulation. Furthermore, the VDP distribution on the outer mitochondrial membrane was quantitatively evaluated by hierarchical clustering analysis under STORM imaging.

2. Results and discussion

Cy5 fluorescent dye is an ideal photoblinking candidate for STORM microscopy and 1, 3, 2-dithiarsenolane is a useful unit for the covalent binding of VDPs. A piperazine spacer was used as the linker (Fig. 1A). Fluorescent probe **1** was prepared according to previously described protocols [16] (see Supporting Inforamtion for details). Prior to its application in cell imaging, the spectral properties of **1** were studied. First, probe **1** in ethanol showed absorption maxima at 649 nm with a molar extinction coefficient of $2.1 \pm 0.3 \times 10^5$ and emission maxima at 670 nm, respectively (Fig. 1B). The same parameters have also been tested in aqueous solution and similar results were obtained (Table S1 in Supplemental Information). A fluorescence quantum yield of 0.28 in ethanol and 0.18 in aqueous solution was obtained compared to Rhodamine B. Additionally, the photoblinking behavior of a single molecule of **1** was investigated using the home-built dSTORM system. In the absence of an imaging buffer and thiols [7,17], a specimen of **1** was directly illuminated by a laser beam (656 nm, 0.8 kW cm^{-2}) to show marked photoblinking fluorescence with a high photon number (*ca.* 3000 photons per pixel at each frame of the fluorescent state in the "on" cycle) and a low on-off duty cycle (*ca.* 0.0013). The mechanism of photoblinking under laser illumination was further discussed in the Supplemental Information (Supplementary Scheme 2). The duration of photoblinking lasts for more than 900 s with a suitable switching frequency, while the average photoblinking cycle of "on" state was approximately 88.2 ms (Fig. 1C–F and Fig. S1).

To evaluate the analytical results of the CSSTORM reconstruction

after NC-PCA de-noising and K-factor sharpening, a fluorescent probe was placed on a coverslip to produce photoblinking under laser illumination at 656 nm. The blinking dataset was analyzed by NC-PCA using different major principal components, as shown in Fig. S17. Comparisons of 1–3 to 1–6 major principal components showed that the fewer principal components chosen for signal reconstruction, the more evident the noise reduction and the higher the potential for signal distortion. 1–6 major principal components were empirically employed to balance noise reduction and the fidelity of the signal in the NC-PCA de-noising process for super-resolution image reconstruction, based on the validation experiments of the NC-PCA algorithm by using simulation data (Figs. S15–S16). When implementing the K-factor algorithm, the parameters M = 54 (number of factors) and h = 9 (number of harmonics) were set manually, and the k value was set automatically, gradually reducing according to the number of factors. The detailed workflow is presented in Fig. S14.

To further verify de-noising by NC-PCA + K-factor treatment prior to CSSTORM localization, we compared the reconstruction results obtained by CSSTORM with those of the single-molecule fitting (insight3 software) algorithm, as shown in Fig. 2, using tubulin with high-density labeling STORM data obtained from an openly available EPFL website [18]. The dataset was first de-noised using the NC-PCA algorithm and then sharpened using the K-factor algorithm. Similar structures of tubulins were obtained by CSSTORM (Fig. 2A (a-c) and single-molecule fitting (Fig. 2A (d)), and CSSTORM exhibited greater structural continuity using only 500 camera frames, and even as few as 200 frames; however, poor continuity was observed when using 100 frames, in a comparison between CSSTORM (Fig. 2A (e-g, i-k, m-o)) and the insight3 algorithm (Fig. 2A (h, l, p)). The magnified view in Fig. 2A (a-d) shows markedly sharpened structures upon de-noising using the NC-PCA + K-factor algorithm (Fig. 2A (g)), which maintained the most structural consistency with the insight3 results (Fig. 2A (h)). Seven microtubules were distinguishable after NC-PCA + K-factor treatment, and ambiguous noisy peaks inevitably appeared between adjacent microtubules in CSSTORM treatment of raw data or for K-factor treatment only, as shown by the dashed circles in Fig. 2B (a-b). Fourier ring correlation (FRC) is a quantitative imaging-resolution measuring tool that has been used to further evaluate improvements in image resolution [19]. Image resolution (R) was determined by the inverse of the spatial frequency indicated by the intersection of the FRC curve with a given threshold, which was empirically set to 1/7 (Fig. S18). NC-PCA + K-factor treatment resulted in the highest imaging resolution of 39 nm, which was comparable to those obtained by CSSTORM for raw data (66 nm) and K-factor only (62 nm).

The biological behavior of probe **1**, including colocalization, covalent binding identification, and cytotoxicity, was studied. The results demonstrated that probe **1** preferentially targeted mitochondria, demonstrated through the optimal merging imaging with Mito-tracker over Lyso-, ER-trackers (Figs. S2A, S3 and S4). Moreover, mitochondrial VDPs were covalently labeled by the probe, which was identified by SDS-PAGE and washing-out experiments. The probe cannot be removed from mitochondria after washing with PBS, PBS-ethanol, or ethanol solvents, (Figs. S2B, S2C, S2D, S5 and S6). Furthermore, the probe showed no cellular toxicity under our experimental conditions (Fig. S7), which is favorable for live cell super-resolution imaging (Fig. 3 and S8).

To identify the exact location of **1** in mitochondria of live cells, STORM super-resolution imaging was performed to determine the ultrafine structure of mitochondria labeled by **1**. Probe **1** (1 μM) was incubated with HeLa cells for 1 h without further treatment and importantly this procedure was simpler than that using Alexa647. Subsequently, the cell samples were fixed with glutaraldehyde before imaging or used for live cell imaging by the STORM system. As shown in Fig. 3A (a), unlike the wide-field image, which cannot provide the fine structure of mitochondria, the super-resolution images showed detailed structures, which were reconstructed using 200 frames by CSSTORM (Fig. 3A (b)) and de-noised CSSTORM in live HeLa cells
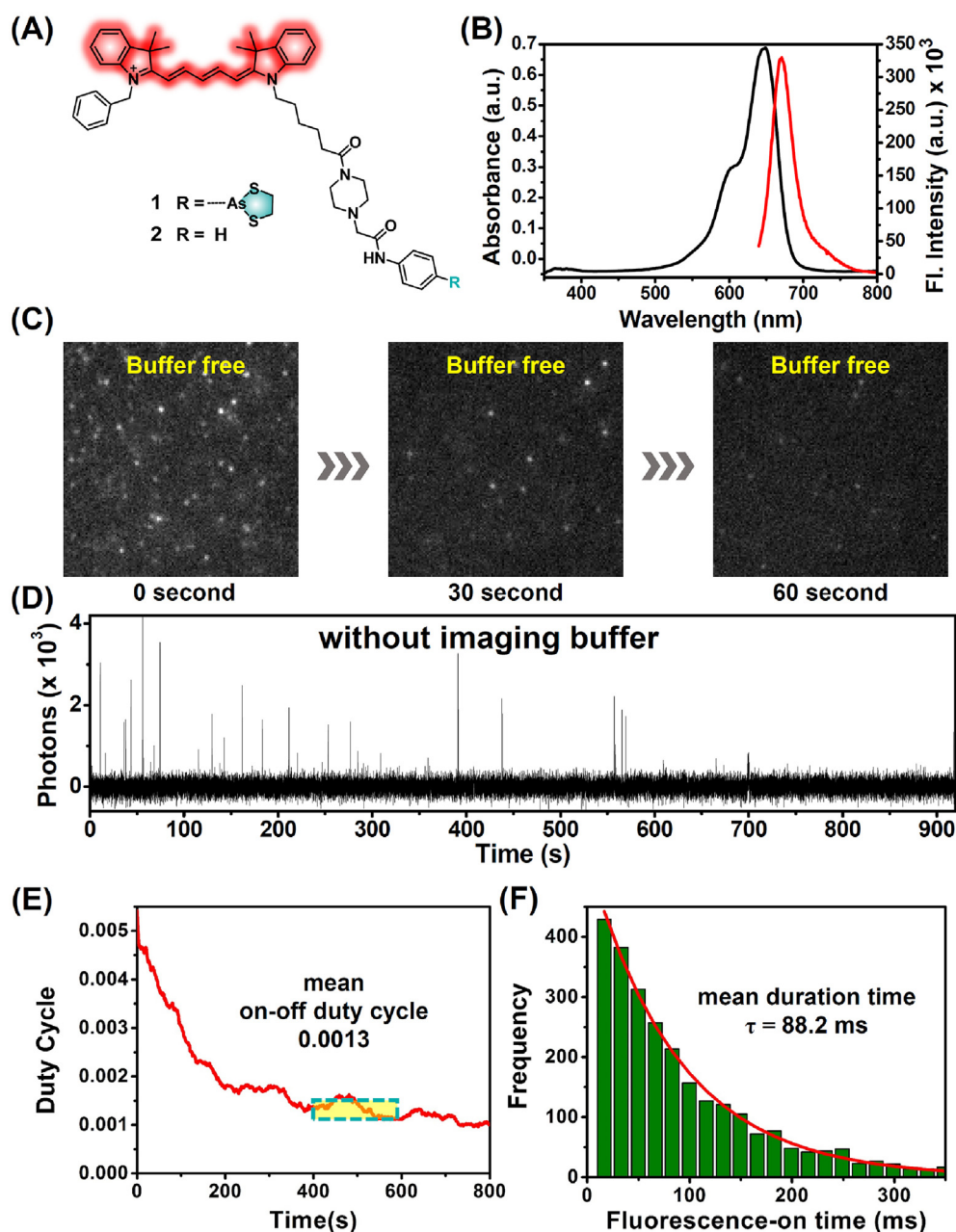
Fig. 1. Chemical structures and optical properties of target compound **1** without imaging buffer. (A) Chemical structure of target compound **1**; (B) Absorption (black) and emission (red) spectra of **1** in ethanol solution; (C) Reversible and spontaneous fluorescence blinking over tens of seconds in the absence of a STORM imaging buffer containing β-mercaptoethanol (BME) and glucose oxidase (GLOX), excited at 656 nm with a laser power of 0.8 kW cm^{-2}; (D) Time traces of single-molecule fluorescence of probe **1**; (E) The on-off duty cycle value was calculated as the fraction of time spent in the on state averaged over many molecules using a sliding window of 100 s, the mean duty cycle was measured between 400 and 600 s indicated by yellow box; (F) Distribution of fluorescence-on time of probe **1**, the indicated mean duration time of 88.2 ms was derived from the single exponential fit (red curve) of the histogram.

(Fig. 3A (c)) or in fixed cells (Fig. 3B). From the magnified image of the region of interest, indicated by dashed square in Fig. 3A (c), the denoised CSSTORM resolution was evidently higher than that of CSSTORM (Fig. 3A (d)), and the discrete granule distribution on the mitochondrial membrane was clearly observed in Fig. 3A (e), indicating that probe **1** selectively labeled VDPs on the mitochondrial membrane. The imaging resolutions of CSSTORM and de-noised CSSTORM were calculated by Gaussian fitting, showing full widths at half maximum (FWHM) of 108.7 and 45.7 nm, respectively, as shown in Fig. 3A (f, g). The covalent binding of **1** to VDPs on mitochondrial membranes was further supported by STORM using fixed HeLa cells. When HeLa cells were incubated with **1**, fixed with glutaraldehyde and washed with PBS, similar super-resolution images of mitochondria were obtained by the de-noised CSSTORM algorithm (Fig. 3B (a, c, d)), and the high imaging resolution (30.2 nm in Fig. 3B (e) enabled the study of the distribution of VDPs on the outer mitochondrial membrane as well as their dynamics (Fig. S8).

STORM was further applied to evaluate dynamic mitochondrial changes, including mitochondrial fusion, fission, and tubulation. Videos demonstrating the dynamics were obtained by the CSSTORM or denoised CSSTORM algorithm using 200 camera frames for reconstructions with a step length of 20 frames to obtain a temporal resolution of 0.8 s. The video results clearly revealed a markedly better resolution of the de-noised CSSTORM images compared with those of wide-field images (Fig. 4A) and CSSTORM images (Fig. 4B). After pre-treatment by the NC-PCA + K-factor method, the de-noised CSSTORM analysis demonstrated obvious noise suppression (Video S2), and the ultra-fine imaging of VDPs on mitochondrial membranes was achieved (Fig. 4C, Fig. S8, and Videos S2–S6). Moreover, typical dynamics of mitochondria can be observed to quantify speeds of mitochondrial fusion, fission, and tubulation, which probably reflects the mitochondrial status in biological activities [20,21], Single mitochondrial tubulation and microtubule stretching were captured (dashed square in Fig. 4C), and different time points are shown in Fig. 4D (1–6). The distance during the tubulation retraction was ~746 nm, and finished in 1.2 s (Fig. 4E). The hollow tube diameter (magnified dashed circle in Fig. 4F), as
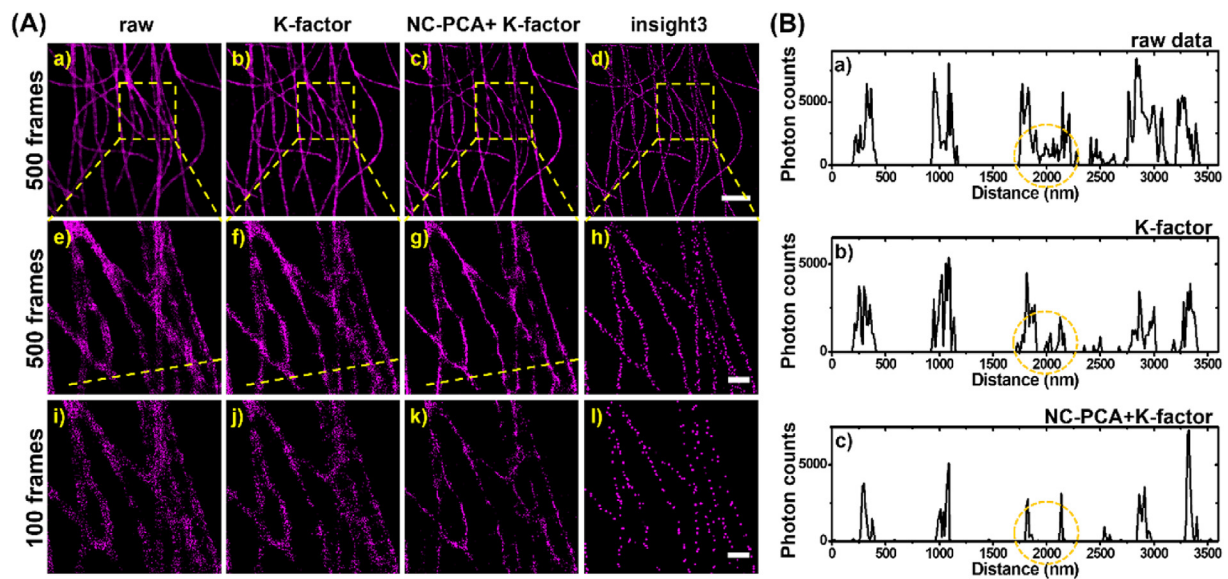
Fig. 2. Validation of the NC-PCA de-noising algorithm using an experimental dataset of tubulins with high-density labeling (from EPFL). (A) Comparison of CSSTORM results for raw data (column 1), K-factor (column 2), and NC-PCA + K-factor pre-treatment (column 3) and single-molecule fitting results (column 4). Row 2–4, magnified view of row 1, reconstructed using 500, 200 and 100 frames, respectively. Scale bar, 2 μm in (d) and 500 nm in (h, l, p); (B) Profiles along the yellow dashed lines shown in (e–g).

calculated by Gaussian fitting, was 51.8 nm, and FWHM values for membrane widths were 46.9 nm and 43.5 nm (Fig. 4G), comparable to previously reported results [22]. Mitochondrial fusion and fission dynamics are shown in Fig. S9 and Videos S3–S8, which have never been achieved by traditional optical microscopy.

Supplementary video related to this article can be found at https://doi.org/10.1016/j.biomaterials.2020.119938.

Studies of the distribution of VDPs on mitochondrial membranes labeled by **1** can provide insight into biological functions. We used the open source software LocAlization Microscopy Analyzer (LAMA) [23] to analyze morphological clusters of VDPs based on density-based hierarchical clustering algorithms, i.e., a density-based algorithm for discovering clusters in large spatial databases with noise (DBSCAN) and ordering points to identify the clustering structure (OPTICS). Considering the pixelation of the compressed sensing algorithm without directly returning a list of molecule coordinates, the CSSTORM results

were first converted to a molecule list as input for LAMA by identifying clusters of nonzero grid points. A region of interest, a 128 × 128 pixels super-resolution grid image, was chosen for the protein clustering analysis (Fig. 5A). The observation radius was set to 19 nm, the minimum cluster size was set to 6 in DBSCAN, and the noise level was set to 13.1% in OPTICS [24]. In total, 32 and 36 clusters were detected by DBSCAN and OPTICS, respectively, and are shown as 2D distributions of cluster populations in Fig. 5 (B, E). A DBSCAN-based hierarchical cluster analysis was performed using the results of DBSCAN or OPTICS to extract morphological information for individual clusters by polygon formation. The morphological cluster analysis results with 16 false colours are summarized in Fig. 5 (C, F). Finally, a cluster population distribution with a cluster size of *ca.* 90 nm was obtained, as shown in Fig. 5 (D, G), indicating that this is a promising strategy for analyses of protein distributions in live cells (Figs. S10–S13).
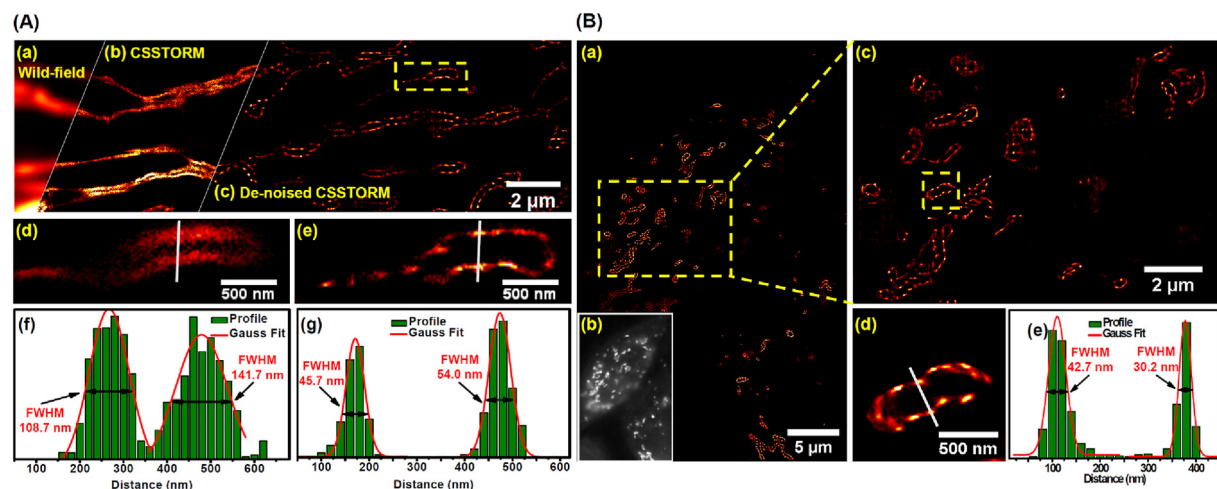

Fig. 3. Super-resolution imaging of mitochondrial membranes labeled with probe **1** in live HeLa cells (A) and in fixed HeLa cells (B). (A) Wide-field fluorescent image (a), and STORM images (b and c) obtained by CSSTORM and de-noised CSSTORM algorithms; (d, e) magnified images of single mitochondria in panel c by CSSTORM and de-noised CSSTORM, respectively; (f, g in A and e in B) Width analysis of the outer membrane; the blue histogram shows the cross-sectional profile along the lines in (d, e) in panel A and (d) in panel B; (B) Wide-field imaging (b); (a, c, d) STORM images obtained by the CSSTORM using 200 frames, EMCCD worked at a frequency of 250 Hz for 64 × 128 pixels raw data acquisition.
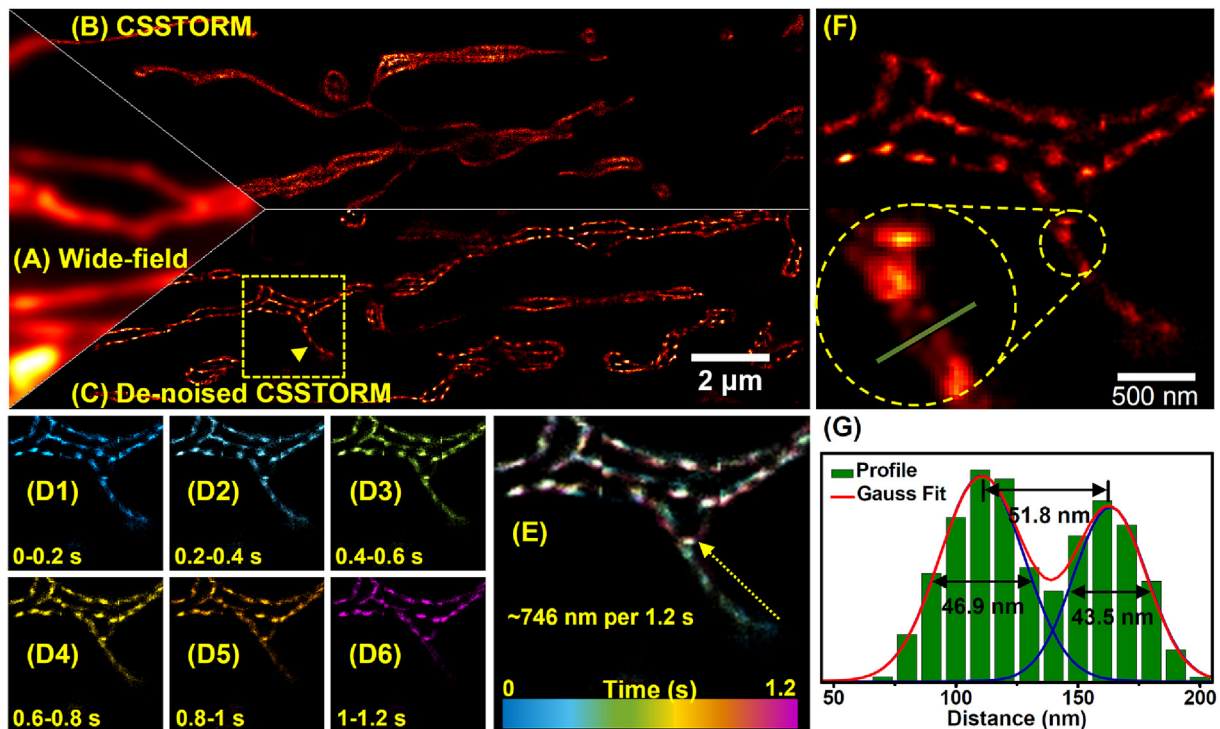
Fig. 4. Mitochondrial tubulation analysis based on super-resolution imaging. (A) Wide-field image of mitochondria; (B, C) Super-resolution images of mitochondria in live HeLa cells analyzed by CSSTORM and de-noised CSSTORM algorithms; (D, E) Mitochondrial tubulation movement, (D1-D6) Different colours represent the movement status of mitochondria at different time points, (E) Whole tubulation retraction process by merging D1-D6; (F) Magnified single mitochondria and stretching tubule in (C); (G) Width analysis of mitochondrial tubules; blue histogram shows the cross-sectional profile along the line marked in the dashed circle in (F) with FWHM values obtained from Gaussian fitting (red and green).
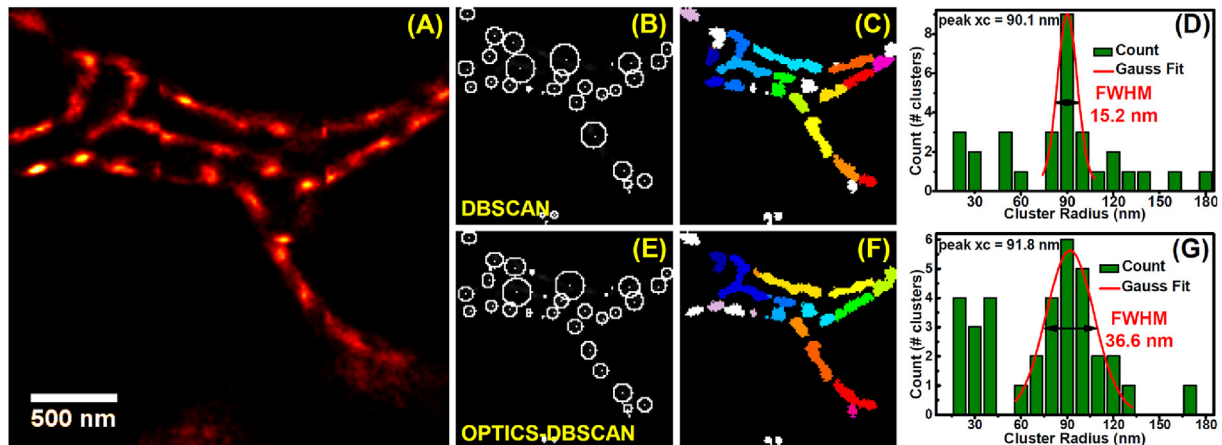

Fig. 5. Distribution of mitochondrial membrane VDPs determined by a protein clustering analysis-using DBSCAN (B, C, D) and OPTICS (E, F, G). (A) STORM super-resolution image (scale bar 500 nm); (B, E) 2D distribution of the cluster population; (C, F) Visual representation of the DBSCAN-based morphological cluster analysis; (D, G) Distribution of cluster radii.

3. Conclusion

In conclusion, a promising strategy for STORM super-resolution microscopy was developed to carry out mitochondrial dynamics imaging in live cells. In this method, a new STORM probe was applied to covalently bind to VDPs in the mitochondrial outer membrane, which achieved STORM super-resolution imaging without the need for an imaging buffer and thiols. The mitochondrial dynamics analyses were obtained by CSSTORM imaging using a noise-correction method consisting of a NC-PCA + K-factor pre-treatment. De-noising CSSTORM enabled ultra-fine structural imaging of mitochondria with a spatial resolution of up to 30.2 nm in fixed cells and 45.7 in live cells with a temporal resolution of 0.8 s. The dynamic changes of the 1-VDP complex on the mitochondrial membrane were utilized to demonstrate mitochondrial dynamics, including fusion, fission, and tubulation, in particular, dynamic tubulation retraction of ca. 746 nm in 1.2 s. The distribution of VDPs on the outer mitochondrial membrane was further analyzed as protein aggregation (*ca.* 90 nm) to gain a deeper insight into their biological functions. The newly developed strategy will be useful for further functional studies of mitochondria.

Declaration of competing interest

The authors declare that they have no known competing financial

interests or personal relationships that could have appeared to influence the work reported in this paper.

Acknowledgements

Appendix A. Supplementary data

Supplementary data to this article can be found online at https://doi.org/10.1016/j.biomaterials.2020.119938.

References

[1] J. Nunnari, A. Suomalainen, Cell 148 (2012) 1145–1159.
[2] S. Meeusen, J.M. McCaffery, J. Nunnari, Science 305 (2004) 1747–1752.
[3] C. Wang, W. Du, Q.P. Su, M. Zhu, P. Feng, Y. Li, Y. Zhou, N. Mi, Y. Zhu, D. Jiang, S. Zhang, Z. Zhang, Y. Sun, L. Yu, Cell Res. 25 (2015) 1108–1120.
[4] D.C. Chan, Annu. Rev. Genet. 46 (2012) 265–287.
[5] H. Chen, D.C. Chan, Hum. Mol. Genet. 18 (2009) 169–176.
[6] H. Zhu, J. Fan, J. Du, X. Peng, Acc. Chem. Res. 49 (2016) 2115–2126.
[7] a) S.A. Jones, S.H. Shim, J. He, X. Zhuang, Nat. Methods 8 (2011) 499–508;
b) S.-N. Uno, M. Kamiya, T. Yoshihara, K. Sugawara, K. Okabe, M.C. Tarhan, H. Fujita, T. Funatsu, Y. Okada, S. Tobita, Y. Urano, Nat. Chem. 6 (2014) 681–689;
c) A. Small, S. Stahlheber, Nat. Methods 11 (2014) 267–279;
d) S. Alexey, R.M. Hochstrasser, Proc. Natl. Acad. Sci. U.S.A. 103 (2006) 18911–18916;
e) R. Iinuma, Y. Ke, R. Jungmann, T. Schlichthaerle, J.B. Woehrstein, P. Yin, Science 344 (2014) 65–69.
[8] Y. Doksani, J.Y. Wu, T. de Lange, X. Zhuang, Cell 155 (2013) 345–356.
[9] a) M. Bates, B. Huang, G.T. Dempsey, X. Zhuang, Science 317 (2007) 1749–1753;
b) B. Huang, W. Wang, M. Bates, X. Zhuang, Science 319 (2008) 810–813.
[10] S. Shen, X.-F. Li, W.R. Cullen, M. Weinfeld, X.C. Le, Chem. Rev. 113 (2013) 7769–7792.
[11] C. Huang, Q. Yin, W. Zhu, Y. Yang, X. Wang, X. Qian, Y. Xu, Angew. Chem. Int. Ed. 50 (2011) 7551–7556.
[12] a) L. Zhu, W. Zhang, D. Elnatan, B. Huang, Nat. Methods 9 (2012) 721–723;
b) J. Huang, K. Gumpper, Y. Chi, M. Sun, J. Ma, Opt. Lett. 40 (2015) 2989–2992.
[13] S.H. Shim, C. Xia, G. Zhong, H.P. Babcock, J.C. Vaughan, B. Huang, X. Wang, C. Xu, G.Q. Bi, X. Zhuang, Proc. Natl. Acad. Sci. U.S.A. 109 (2012) 13978–13983.
[14] X. Peng, Z. Yang, J. Wang, J. Fan, Y. He, F. Song, B. Wang, S. Sun, J. Qu, J. Qi, M. Yan, J. Am. Chem. Soc. 133 (2011) 6626–6635.
[15] S.N. Uno, M. Kamiya, T. Yoshihara, K. Sugawara, K. Okabe, M.C. Tarhan, H. Fujita, T. Funatsu, Y. Okada, S. Tobita, Y. Urano, Nat. Chem. 6 (2014) 681–689.
[16] http://bigwww.epfl.ch/smlm/datasets/.
[17] R.P. Nieuwenhuizen, K.A. Lidke, M. Bates, D.L. Puig, D. Grunwald, S. Stallinga, B. Rieger, Nat. Methods 10 (2013) 557–562.
[18] a) P. Mishra, D.C. Chan, J. Cell Biol. 212 (2016) 379–387;
b) D. Sebastian, M. Palacin, A. Zorzano, Trends Mol. Med. 23 (2017) 201–215.
[19] M. Lavorato, V.R. Iyer, W. Dewight, R.R. Cupo, V. Debattisti, L. Gomez, S. De la Fuente, Y.-T. Zhao, H.H. Valdivia, G. Hajnoczky, C. Franzini-Armstrong, Proc. Natl. Acad. Sci. U.S.A. 114 (2017) 849–858.
[20] P.R. Nicovich, D.M. Owen, K. Gaus, Nat. Protoc. 12 (2017) 453–460.
[21] S. Jahirabadkar, P. Kulkarni, Expert Syst. Appl. 41 (2014) 2939–2946.
[22] Y. Wang, S. Jia, H.F. Zhang, D. Kim, H. Babcock, X. Zhuang, L. Ying, Optica 4 (2017) 1277–1284.
[23] P.R. Nicovich, D.M. Owen, K. Gaus, Nat. Protoc. 12 (2017) 453–460.
[24] S.J. Holden, S. Uphoff, A.N. Kapanidis, Nat. Methods 8 (2011) 279–280.